Numerical simulation of humidification and heating during inspiration within an adult nose*

Fabian Sommer[1], Ralf Kröger[2], Jörg Lindemann[1]

[1] Department of Otorhinolaryngology, Head and Neck Surgery, University Hospital Ulm, Ulm, Germany

[2] ANSYS Germany GmbH, Darmstadt, Germany

Rhinology 50: 157-164, 2012

DOI:10.4193/Rhino11.231

***Received for publication:**

October 30, 2011

Accepted: December 19, 2011

Background: The temperature of inhaled air is highly relevant for the humidification process. Narrow anatomical conditions limit possibilities for in vivo measurements. Numerical simulations offer a great potential to examine the function of the human nose.

Objective: In the present study, the nasal humidification of inhaled air was simulated simultaneously with temperature distribution during a respiratory cycle.

Methods: A realistic nose model based on a multislice CT scan was created. The simulation was performed by the Software Fluent®. Boundary conditions were based on previous in vivo measurements. Inhaled air had a temperature of 20°C and relative humidity of 30%. The wall temperature was assumed to be variable from 34°C to 30°C with constant humidity saturation of 100% during the respiratory cycle.

Results: A substantial increase in temperature and humidity can be observed after passing the nasal valve area. Areas with high speed air flow, e.g. the space around the turbinates, show an intensive humidification and heating potential. Inspired air reaches 95% humidity and 28°C within the nasopharynx.

Conclusion: The human nose features an enormous humidification and heating capability. Warming and humidification are dependent on each other and show a similar spacial pattern. Concerning the climatisation function, the middle turbinate is of high importance. In contrast to in vivo measurements, numerical simulations can explore the impact of airflow distribution on nasal air conditioning. They are an effective method to investigate nasal pathologies and impacts of surgical procedures.

Key words: numerical simulation, humidification, CFD, heating, inspiration, respiratory cycle

Introduction

The main function of the human nose is conditioning of inhaled air, which enables an optimal gas exchange in the lower respiratory tract. Especially the anterior nasal segment is of particular importance as presented by former in vivo studies [(1,2)]. The inspired airstream gets - similar to a jet nozzle - compressed and accelerated. After passing the nasal valve it is disrupted, slowed down and dispersed consecutively. Dispersion and hence turbulences created by this barrier within the airstream enable the mucosa to transfer heat and moisture to the inhaled air due to a close contact between air and nasal wall [(3)]. Nasal airflow is essential for an adequate climatisation of inhaled air. The increase of air temperature within the anterior nasal segment directly behind the nasal valve area is much more effective than along the rest of the more posterior nasal airways as Keck et al., revealed [(1)]. Differences in temperature between air and mucosa are decisive factors for water transfer from mucosal surface to inhaled air [(3,4)]. Resulting from

an increase in temperature, moisture transport becomes more effective and vice versa.

Various investigations showed that in vivo measurements of temperature and humidity within the centre of the air stream and close to the nasal mucosa [1,5-7] are realizable. However, a limitation of in vivo measurements is the complex anatomical structure and mucosal surface of the human nose. Furthermore, in vivo measurements only allow a limited number of simultaneous measuring points within the anterior nasal cavity. A fundamental problem of in vivo temperature and humidity measurements is the poor spatial and time resolution [8]. Therefore, they are feasible only to a restricted extent exclusively providing single temperature values. Posterior areas as the nasopharynx are accessible only by uncongenial methods for the patient. Therefore, in vivo data on the overall performance of the nose are based on only single measurements within each nasal segment. A simultaneous mapping of the nose is not realizable. However, today´s knowledge of temperature and humidity is based on these studies.

Additionally, in vivo studies on intranasal airflow patterns are technically not practicable due to the size of sensors and connecting cables and their influence on airflow patterns. Mlynski et al., made nasal airflow visible by so called 'nose like models' [9]. They created replicas on the basis of a real cadaver human nose and visualized currents by coloured fluids that passed through these models. However, information on temperature and humidity cannot be achieved by this method.

Here, numerical simulations applying computational fluid dynamics (CFD), offer new techniques. During the last decade, CFD simulation more and more replaced experimental setups especially in the automotive industry, which was realized by more capable computational power and further software development. Numerical simulation nowadays is an efficient tool for displaying real environment (e.g. anatomical structures) within a computational model. Within the last few years, this technique found its way into the medical sector, concerning especially vascular pathologies [10-12]. But also nasal air conditioning can be analysed as a function of airflow patterns [13].

Technical issues led to a large number of CFD projects within the last years providing novel information about the complex functions of human airways [13]. The study group around Lindemann et al., performed CFD simulations of airflow pattern characteristics in combination with intranasal air temperature under various conditions [8,14-18]. CFD is able to visualise the close relationship between intranasal airflow and heat transfer. Changes in temperature are strongly affected by airflow patterns.

Existing CFD studies examined intranasal airflow patterns without providing any information about intranasal heating *and* humidification. Moreover, a steady state inspiration was assumed [19,20]. Numerical simulations applying CFD offer a detailed analysis and visualisation of airflow patterns within the entire nasal cavity even during a respiratory cycle. Therefore airflow patterns like turbulences, vortices, volume flow as well as pressure conditions can be investigated for varying flow rates. Most of up to date studies simulated a static inflow. A CFD simulation of intranasal humidification as a function of temperature and airflow during a dynamic respiratory cycle is not yet published. The humidity exchange between wall and inspired air is difficult to simulate due to complex physiological attributes of the mucosa. Values obtained from own in vivo measurements [3,6] were applied as boundary conditions for the numerical simulation in order to provide preferably physiological conditions.

Material and methods

Model geometry

A computational model of a human nose was constructed by using a CT-Scan of a human nose. A scan of a 39-year old man with approximately regular anatomic conditions was used. The patient had no pathology concerning the paranasal sinuses and no history of nasal disease or allergy. Appropriate fluid flow physics were applied to this virtual model. In the present study flow patterns of air, temperature and moisture distribution within the nasal cavity were simulated.
The CT-scan was performed on a Philips multislice CT Mx8000 with the following parameters: primarily axial layers, slice thickness 1.3 mm; increment 0.6 mm. Segmentation was performed by the commercial Software SURFdriver 3.5.6 (SURFdriver; Kailua, HI, USA). This software traces the contours of each single slice and allows manual correction in case of artifacts or inaccuracy of the algorithm. In order to provide a high mesh quality a slight smoothing algorithm was used. Special care was taken of preserving the original anatomy.
Gambit 1.2 (Fluent Inc.; Lebanon, NH, USA) conducted the post-processing of the model geometry. In the end an unstructured tetrahedral mesh with 401.000 cells was constructed around the surface model (Figure 1).

Boundary conditions and Simulation

The numerical simulation was performed by the commercial CFD solver Fluent 5.5.14 (Fluent Inc., (present-day ANSYS)). This simulation is based on the numerical solution of the Navier-Stokes equation, which represents a general equation for three-dimensional flow of compressible and viscous fluids.
The boundary conditions were based on own in vivo measurements. In these experiments, small sensors were inserted in the nasal cavity and a temperature and humidity profile of the

nasal wall was defined. According to these results, boundary conditions were defined as follows: The breathing cycle had a frequency of 14.3 gasps per minute with inspiration taking 1.9 seconds and expiration 2.3 seconds (4.2 seconds for one complete cycle) representing a quiet respiration frequency. Three whole cycles were included in the simulation. In contrast to most existing studies no steady state inspiration was assumed. Based on previous in vivo measurements, which examined intranasal pressure and inspired volume, a dynamic breathing cycle was simulated. Assuming a quiet breathing cycle, the maximum inspiratory airspeed was 0.9 meters per second. Figure 2 describes the simulated cycles. The median tidal volume was 312 ml. Inspired air was simulated at 20°C and 30% relative humidity. During inspiration the temperature of the wall was assumed to decrease from 34°C to 30°C at the end of the cycle, according to results of previous experiments [3,6]. Expiration led to an increase from 30°C to 34°C. The moisture content of the nasal mucosa was assumed to be 100% during in- and expiration. This boundary condition was defined assuming that a constant mucus film covers the nasal wall during quiet breathing. Expired air (lung) had a temperature of 35°C and a relative humidity of 100%. To simulate the influence of the nasal alars and skin the external nose was added to the model. External skin temperature of the nose was constantly at 31°C. The velocity inlet was defined to be a spherical structure around the external nose (Figure 3). Coronary slices at representative locations within the nose model were chosen to display the humidity dispersion over the three-dimensional volume model (Figure 4).

Results

The inspiratory humidification is graphically presented in Figure 5 and Figure 6. Red colour indicates a humidity saturation of 100%. Lower values are represented by colours as listed on the sinistral scale. A surface plot was calculated to illustrate the water vapour concentration of a layer directly adjacent to the geometry wall (Figure 7). Yellow indicates the constant concentration of the wall (100%) whereas blue stands for lower values. It is clearly demonstrated that most of the humidity of the mucosa is transferred to the inspired air within the anterior third of the nasal passage.

Due to changing velocities according to the simulated breathing cycle, three different diagrams illustrating temperature and humidity were chosen to visualize the results. Measuring points were 0.5 seconds after beginning of inspiration (increasing velocity), 1 second (representing the maximum flow) and 1.4 seconds after beginning of inspiration (representing decreasing velocity). Figure 6 illustrates the humidity dispersion during maximum inspiration on the left side and temperature distribution on the right side. Inspired air at the nasopharynx reached up to 95% relative humidity (98% after 0.5 seconds and 96% after 1.4 seconds) even during maximum inspiration. Temperature reached 28°C during maximum inspiration (32°C after 0.5 seconds and 27°C after 1.4 seconds). The humidity increase was even higher (98% and 97%) for lower airspeeds (at 0.5 and 1.4 seconds with a flow rate of 0.55 meters per second). Temperature increase was higher during the beginning of inspiration (32°C) and lower at the end of inspiration (27°C) as a result of the decreasing temperature of the nasal wall during inspiration. A particularly rapid increase in temperature and humidity could be observed after passing the nasal valve area and the anterior third of the nasal cavity. Regarding the flow rate of inspired air, the inferior nasal passage and the nasal roof area had no essential effect. The velocity did not exceed 0.04 m/s in these areas.

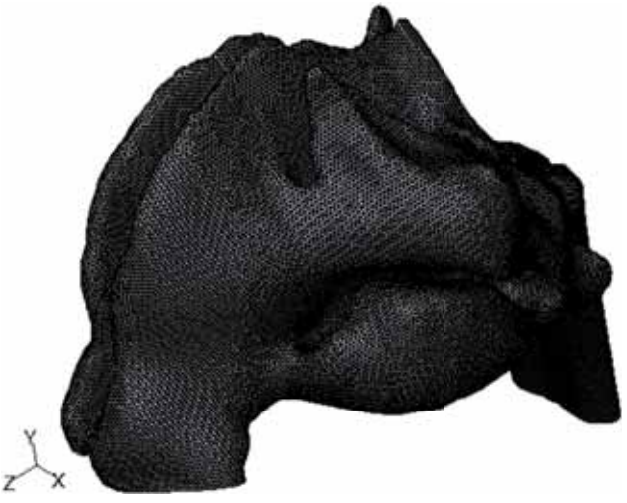

Figure 1. Tetrahedral mesh created from a CT scan.

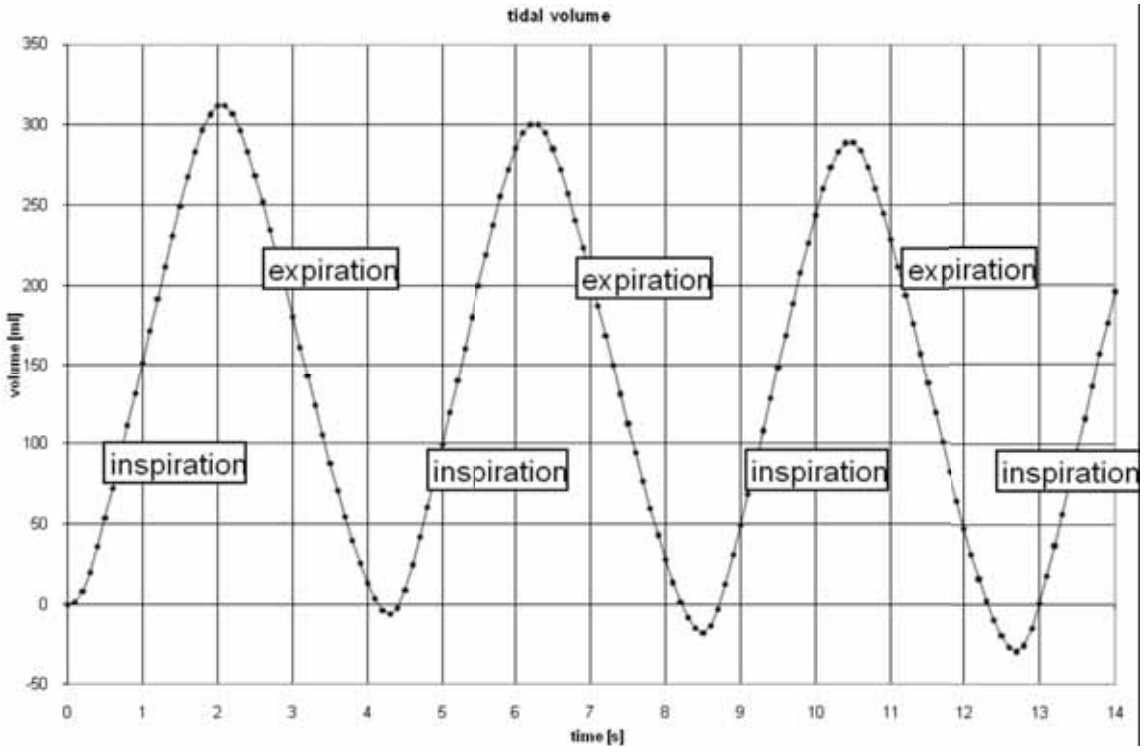

Figure 2. Tidal volume of the simulated breathing cycle.

During inspiration most of the inhaled air was dispersed and consecutively saturated up to a relative humidity of 90 % by passing the nasal valve area and as well as the middle turbinate area. The area with the lowest water vapour saturation can be found between the nasal valve area and the head of the middle turbinate as demonstrated in Figure 7. Immediately after passing the anterior part of the middle turbinate humidity and temperature increase rapidly.

The region around the inferior turbinate provide for a high influence on humidification and heating. Here the inspiratory airstream gets disrupted and diverted. Additionally the cross sectional area grows which leads to a slower airstream and an extended contact to the mucosa.
Additionally, the nasal roof- and floor-area present a continuous saturation of nearly 100% during inspiration. Areas with high-speed air-flow, e.g. the narrow space between septum and medial part of the medial turbinate, show a deferred humidification. Areas with lower airspeed present a higher saturation percentage.

Discussion

The human nose is a small but very complex anatomical organ with important and yet partially unknown functions. Heating, humidification and cleaning of inspired air are the most fundamental tasks. Different experimental set ups were applied to simulate currents and fluid dynamics within the human nose.

Due to fast increase of computational processing power within the last 10 to 15 years numerical simulation became increasingly important concerning medical purposes. Fundamental research for exploration of boundary conditions by means of in vivo measurements was necessary to adopt CFD for rhinologic purposes [13]. However, a simulation of all air-conditioning functions (heating, humidification, cleaning) of the human nose remains a challenging task. This is mainly caused by the coherence of temperature, pressure and resulting wall dynamics, vortices and humidity saturation. To allow for all these boundary conditions the simulation grows complex and computationally intensive. Especially breathing cycle dependent dynamics and resulting changes within the mesh demand high computational power.

First simulations of intranasal temperature changes showed convincing results compared to our previous in vivo measurements [8,14,15,18]. Further studies demonstrated intranasal temperature changes during breathing cycle, particle deposition, effects of sinus surgery, turbinoplasty and atrophic rhinitis [5,20-22] with high spatial resolution. Beside nasal airflow also warming and the consequences of operative procedures were spotlighted [23,24]. Chen et al., described the heat transfer to inspired air for different configurations of inferior turbinate surgery. Humidity transfer was not examined. Additionally, a static inflow was chosen. Naftali et al., performed a simulation using a breathing cycle assuming a static nasal wall tempera-

Figure 3. Velocity inlet defined as spherical structure.

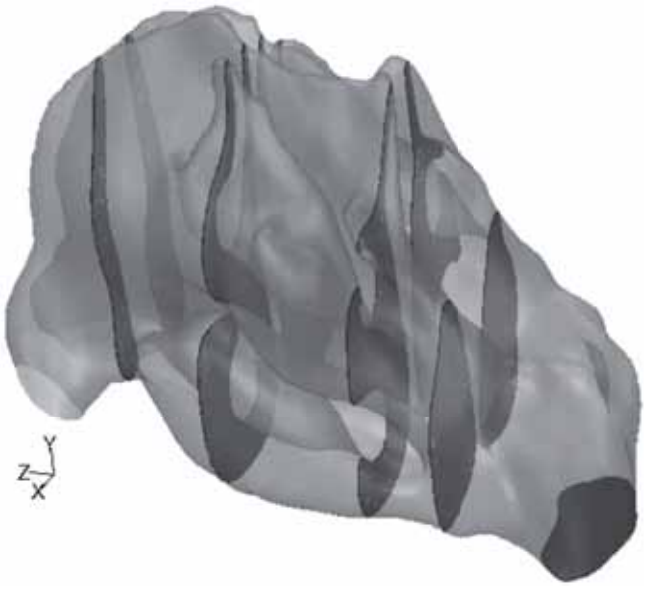

Figure 4. Position of coronary slices within the mesh.

ture [25]. As our in vivo measurement showed, the wall temperature decreases during inspiration which reduces its heating and subsequently humidification capacity.

Of course, boundary conditions are approximations to physiological in vivo measurements. To provide for preferably physiological conditions, values from own in vivo measurements were applied as boundary conditions for the numerical simulation (respiratory volume, flow velocity, nasal wall temperature, air temperature, wall conditions, etc.). However, active processes of the nasal mucosa such as secretion of mucous glands, mucociliary clearance, fluid lining consisting of sol and gel phase, vascular perfusion, congestion and decongestion of the turbinates, etc. cannot be simulated.

To reduce computing time a static wall was chosen in our model. In the present simulation mucosal temperature was simulated to be variable regulated by in- and expiration. Furthermore, the humidity saturation of the nasal wall was defined to be 100% continuously. Assuming a constant film of mucus during quiet respiration this presumption seemed realistic for a quiet breathing cycle. Due to the dynamic airflow three representative points in time (each with different airspeed) were chosen in order to visualize the humidification process. The most remarkable humidification load occurs during maximum inspiration, which is depicted in Figure 6. Humidification and temperature reached even higher values for lower airspeeds as a result of prolonged contact time with the nasal mucosa (Figure 5).

The presented results were identical to previous in vivo measurements. Furthermore, they emphasize the significance of the anterior nasal segment including the nasal valve area. Heating and humidification of inspired air take place in the same regions and are dependent on each other. Analogue to temperature increase, humidification experiences the maximum increase after passing the nasal valve area. Regions with low velocities show nearly constant temperature and a high grade of humidity even during maximum inspiration. Sections with narrow diameters and high speed airflow showed a deferred humidification. Interestingly, the main part of the airstream does not affect the inferior turbinate although it provides a large mucosal surface area within the nasal cavity. However, as an immediate neighbour to the main airstream it acts as a heat and moisture reservoir. This is clearly demonstrated in Figure 5 and Figure 6 as temperature along the inferior turbinate also decreases significantly during inspiration. Additionally, it is a part of the nasal valve and hence responsible for dispersion of inspired air.

Presented results are relative values, dependent on the boundary conditions of inspired air. Anyhow, regions that are mainly responsible for the climatisation maintain its function even for different temperature values of inspired air. The

Figure 5. Humidity (upper row) and temperature (lower row) dispersion during beginning of inspiration.

Figure 6. Humidity (upper row) and temperature (lower row) dispersion during maximum inspiration.

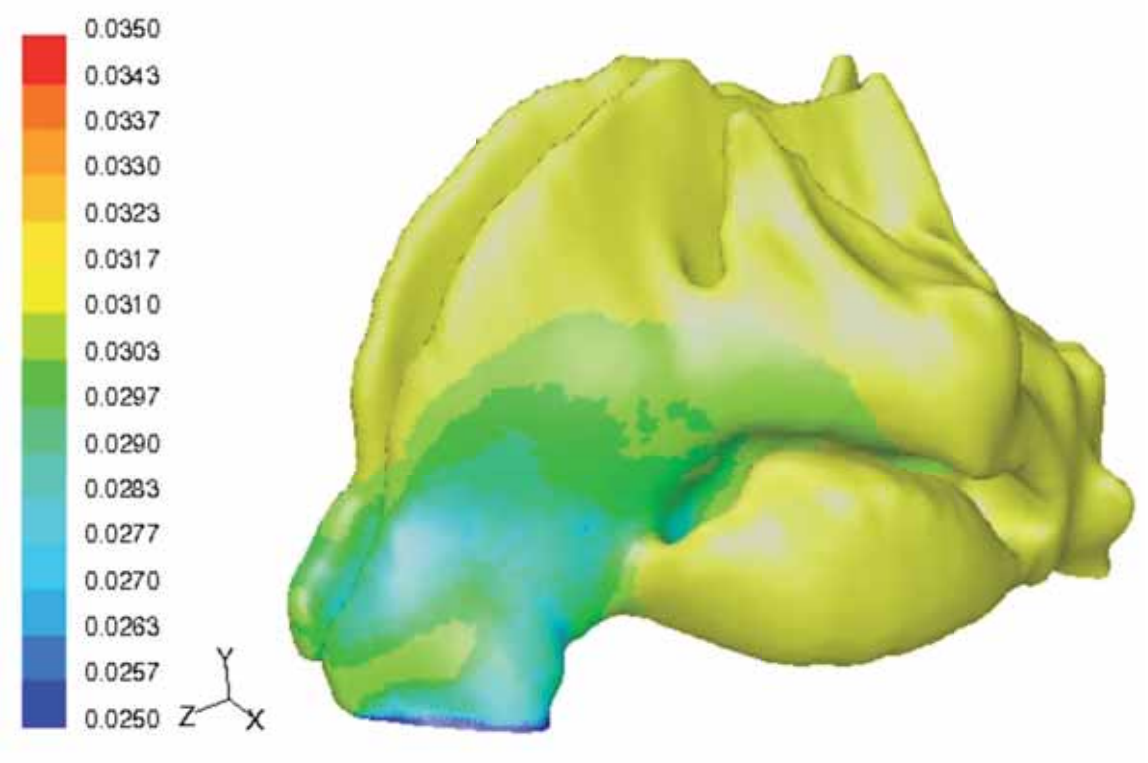

Figure 7. Contours of mass fraction of H_2O.

anterior nasal segment with its function as diffuser is of crucial importance for the nasal 'climate control function.' It reduces the speed of inhaled air by increasing the cross sectional area. Moreover, the nasal valve disperses the airstream preferably equably along the whole cross sectional area. This leads to a prolonged contact time with the nasal mucosa even in regions with high-speed airflow. As a consequence, a distinct increase in air temperature and humidity occurs. Although our results are based on a computer simulation, their significance is underlined by the accordance with existing in vivo measurements of intranasal heating and humidification [3,6,26].

Conclusion

The human nose features very efficient humidification and heating system. During quiet breathing, a humidification up to almost 100% and an increase of temperature up to 28°C (based on an external air temperature of 20°C) during inspiration is performed due to a close contact between air and nasal mucosa.

Simulation of humidification and heating by means of Computational Fluid Dynamics is a highly effective method for investigating the human nose. Due to complex anatomy in limited spatial conditions even small changes can have serious impact on the climatisation and cleaning function of the nose.

In contrast to in vivo measurements, very small changes of boundary conditions (humidity, temperature and anatomy) can be simulated and their effects on all areas of the nose can be investigated. The coherence of dispersion and velocity of inspired air, temperature and its effect on humidification can be visualized. This allows for a profound understanding of the physiology of the human nose. Numerical simulations can explain physiological processes within the nose more detailed than in vivo measurements. Therefore, they are a helpful tool to examine effects of surgery on the 'human climatisation system.'

Conflict of interest statement

All authors have read and approved the submission of the manuscript. The manuscript has not been published and is not being considered for publication elsewhere, in whole or in part or in any language. None of the authors have financial or other kinds of interests that might pose a conflict of interest in connection with the submitted article.

References

1. Keck T, Leiacker R, Riechelmann H, Rettinger G. Temperature profile in the nasal cavity. Laryngoscope. 2000; 110: 651-654.
2. Keck T, Leiacker R, Heinrich A, Kuhnemann S, Rettinger G. Humidity and temperature profile in the nasal cavity. Rhinology. 2000; 38: 167-171.
3. Wiesmiller K, Keck T, Leiacker R, Lindemann J. Simultaneous in vivo measurements of intranasal air and mucosal temperature. Eur Arch Otorhinolaryngol. 2007; 264: 615-619.
4. Keck T, Leiacker R, Riechelmann H, Rettinger G. Temperature profile in the nasal cavity. Laryngoscope. 2000; 110: 651-654.
5. Wiesmiller K, Keck T, Leiacker R, Lindemann J. Simultaneous in vivo measurements of intranasal air and mucosal temperature. Eur Arch Otorhinolaryngol. 2007; 264: 615-619.
6. Walker JE, Wells RE, Jr., Merrill EW. Heat and water exchange in the respiratory tract. Am J Med. 1961; 30: 259-267.
7. Keck T, Leiacker R, Riechelmann H, Rettinger G. Temperature profile in the nasal cavity. Laryngoscope. 2000; 110: 651-654.
8. Lindemann J, Leiacker R, Sikora T, Rettinger G, Keck T. Impact of unilateral sinus surgery with resection of the turbinates by means of midfacial degloving on nasal air conditioning. Laryngoscope. 2002; 112: 2062-2066.
9. Lindemann J, Leiacker R, Rettinger G, Keck T. Nasal mucosal temperature during respiration. Clin Otolaryngol Allied Sci. 2002; 27: 135-139.
10. Wiesmiller K, Keck T, Rettinger G, Leiacker R, Dzida R, Lindemann J. Nasal air conditioning in patients before and after septoplasty with bilateral turbinoplasty. Laryngoscope. 2006; 116: 890-894.
11. Lindemann J, Keck T, Wiesmiller K, Sander B, Brambs HJ, Rettinger G et al. A numerical simulation of intranasal air temperature during inspiration. Laryngoscope. 2004; 114: 1037-1041.
12. Mlynski G, Grutzenmacher S, Plontke S, Mlynski B, Lang C. Correlation of nasal morphology and respiratory function. Rhinology. 2001; 39: 197-201.
13. Kiousis DE, Wulff AR, Holzapfel GA. Experimental studies and numerical analysis of the inflation and interaction of vascular balloon catheter-stent systems. Ann Biomed Eng. 2009; 37: 315-330.
14. Kiousis DE, Gasser TC, Holzapfel GA. A numerical model to study the interaction of vascular stents with human atherosclerotic lesions. Ann Biomed Eng. 2007; 35: 1857-1869.
15. Marchandise E, Willemet M, Lacroix V. A numerical hemodynamic tool for predictive vascular surgery. Med Eng Phys. 2009; 31: 131-144.
16. Keck T, Lindemann J. [Simulation and air-conditioning in the nose]. Laryngorhinootologie. 2010; 89 Suppl 1:S1-14.
17. Lindemann J, Keck T, Wiesmiller K, Sander B, Brambs HJ, Rettinger G et al. A numerical simulation of intranasal air temperature during inspiration. Laryngoscope. 2004; 114: 1037-1041.
18. Pless D, Keck T, Wiesmiller K, Rettinger G, Aschoff AJ, Fleiter TR et al. Numerical simulation of air temperature and airflow patterns in the human nose during expiration. Clin Otolaryngol Allied Sci. 2004; 29: 642-647.
19. Lindemann J, Keck T, Wiesmiller KM, Rettinger G, Brambs HJ, Pless D. Numerical simulation of intranasal air flow and temperature after resection of the turbinates. Rhinology. 2005; 43: 24-28.
20. Lindemann J, Keck T, Wiesmiller K, Sander B, Brambs HJ, Rettinger G et al. Nasal air temperature and airflow during respiration in numerical simulation based on multislice computed tomography scan. Am J Rhinol. 2006; 20: 219-223.
21. Lindemann J, Brambs HJ, Keck T, Wiesmiller KM, Rettinger G, Pless D. Numerical simulation of intranasal airflow after radical sinus surgery. Am J Otolaryngol. 2005; 26: 175-180.
22. Pless D, Keck T, Wiesmiller KM, Lamche R, Aschoff AJ, Lindemann J. Numerical simulation of airflow patterns and air temperature distribution during inspiration in a nose model with septal perforation. Am J Rhinol. 2004; 18: 357-362.
23. Croce C, Fodil R, Durand M, Sbirlea-Apiou G, Caillibotte G, Papon JF et al. In vitro experiments and numerical simulations of airflow in realistic nasal airway geometry. Ann Biomed Eng. 2006; 34: 997-1007.
24. Garcia GJ, Bailie N, Martins DA, Kimbell JS. Atrophic rhinitis: a CFD study of air conditioning in the nasal cavity. J Appl Physiol. 2007; 103: 1082-1092.
25. Keck T, Lindemann J. [Simulation and air-conditioning in the nose]. Laryngorhinootologie 2010; 89 Suppl 1:S1-14.
26. Lindemann J, Keck T, Wiesmiller K, et al. A numerical simulation of intranasal air temperature during inspiration. Laryngoscope. 2004; 114: 1037-1041.
27. Pless D, Keck T, Wiesmiller K, et al. Numerical simulation of air temperature and airflow patterns in the human nose during expiration. Clin Otolaryngol Allied Sci. 2004; 29: 642-647.
28. Lindemann J, Keck T, Wiesmiller KM, Rettinger G, Brambs HJ, Pless D. Numerical simulation of intranasal air flow and temperature after resection of the turbinates. Rhinology. 2005; 43: 24-28.
29. Pless D, Keck T, Wiesmiller KM, Lamche R, Aschoff AJ, Lindemann J. Numerical simulation of airflow patterns and air temperature distribution during inspiration in a nose model with septal perforation. Am J Rhinol. 2004; 18: 357-362.
30. Lindemann J, Leiacker R, Sikora T, Rettinger G, Keck T. Impact of unilateral sinus surgery with resection of the turbinates by means of midfacial degloving on nasal air conditioning. Laryngoscope. 2002; 112: 2062-2066.
31. Rozsasi A, Leiacker R, Rettinger G, Lindemann J, Keck T. Impact of resection of the turbinates and the lateral nasal wall on particle deposition. Laryngoscope. 2004; 114: 646-651.
32. Wiesmiller K, Keck T, Leiacker R, Sikora T, Rettinger G, Lindemann J. The impact of expiration on particle deposition within the nasal cavity. Clin Otolaryngol Allied Sci. 2003; 28: 304-307.
33. Garcia GJ, Bailie N, Martins DA, Kimbell JS. Atrophic rhinitis: a CFD study of air conditioning in the nasal cavity. J Appl Physiol. 2007; 103: 1082-1092.
34. Lindemann J, Leiacker R, Rettinger G, Keck T. Nasal mucosal temperature during respiration. Clin Otolaryngol Allied Sci. 2002; 27: 135-139.
35. Lindemann J, Sannwald D, Wiesmiller K. Age-related changes in intranasal air conditioning in the elderly. Laryngoscope. 2008; 118: 1472-1475.
36. Wiesmiller K, Keck T, Leiacker R, Lindemann J. Simultaneous in vivo measurements of intranasal air and mucosal temperature. Eur Arch Otorhinolaryngol. 2007; 264: 615-619.

Dr. Fabian Sommer
Department of Otorhinolaryngology
Head and Neck Surgery
University Hospital Ulm
Frauensteige 12
89075 Ulm
Germany